Iranian Journal of Numerical Analysis and Optimization
Vol. 15, No. 3, 2025, pp 952–992
https://doi.org/10.22067/ijnao.2025.92605.1612
https://ijnao.um.ac.ir/

Research Article

Mathematical modeling of COVID-19 spread with media coverage and optimal control analysis

G.P. Sahu and A.S. Thakur*,

Abstract

The COVID-19 pandemic, initiated by the SARS-CoV-2 virus, first emerged in Wuhan, China and quickly propagated worldwide. In India, lacking immediate access to effective vaccines and antiviral drugs, the response primarily relied on nonpharmaceutical interventions. These strategies, extensively covered by the media, were vital in promoting preventive behaviors to limit viral transmission. This research introduces a new mathematical model, $SAEI_aIRUM$, to analyze COVID-19's transmission dynamics. It includes a saturation functional response to depict the media's role in influencing public behavior. The control reproduction number (R_c) is determined, and both local and global stability of the disease-free equilibrium

*Corresponding author

Received 12 March 2025; revised 30 April 2025; accepted 29 May 2025

Govind Prasad Sahu
Center for Basic Sciences, Pt. Ravishankar Shukla University, Raipur, Chhattisgarh. e-mail: govind3012@gmail.com

Amit Singh Thakur
School of Studies in Mathematics, Pt. Ravishankar Shukla University, Raipur, Chhattisgarh. e-mail: amitsinghprsu@gmail.com

How to cite this article
Sahu, G.P. and Thakur, A.S., Mathematical modeling of COVID-19 spread with media coverage and optimal control analysis. *Iran. J. Numer. Anal. Optim.*, 2025; 15(3): 952-992. https://doi.org/10.22067/ijnao.2025.92605.1612

are analyzed. Using the least-squares method, the model fits daily case data from India from March 30, 2020, to January 24, 2021. We evaluate the impact of various control parameters on disease progression through numerical simulations and employ normalized forward sensitivity analysis to identify critical parameters affecting R_c. The study advances by formulating an optimal control problem, incorporating the cost of preventive actions as control variables. Findings indicate that an early optimal control strategy could lessen the severity of epidemic peaks by distributing their effects over a longer duration. Simulations demonstrate that combining four control measures outperforms a single or no control.

AMS subject classifications (2020): Primary 92D30; Secondary 92C60.

Keywords: COVID-19; Environmental transmission; Saturated awareness; Optimal control.

1 Introduction

Coronaviruses are a group of single-stranded, positive-sense RNA viruses classified under the Coronaviridae family [14]. They were first classified in 1960, with the name "corona" inspired by their distinctive crown-like structure observed under a microscope [29]. Over time, these viruses have been responsible for three significant outbreaks: The Severe Acute Respiratory Syndrome (SARS) outbreak in China (2003), the Middle East Respiratory Syndrome (MERS) outbreak in Saudi Arabia (2012) [30], and its resurgence in South Korea (2015) [60].

The World Health Organization (WHO) formally named the illness resulting from the novel coronavirus SARS-Cov-2 as Coronavirus Disease 2019 (COVID-19) [36, 17, 33]. Widely acknowledged as one of the most severe public health crises of the 21st century, the COVID-19 pandemic has exerted profound and widespread effects across the globe. Coronaviruses are RNA-based enveloped viruses known to infect both mammals and birds, frequently causing respiratory infections [51, 59]. Recognizable symptoms such as fever, dry cough, and fatigue became widely acknowledged early in the pandemic [26]. COVID-19 has exhibited a rapid transmission rate and high mortal-

ity, surpassing the severity of SARS and MERS. Beyond its physical impact, the pandemic has inflicted profound psychological distress, contributing to heightened anxiety, loneliness, and reduced resilience. The economic losses attributed to infectious diseases during this period are estimated to have exceeded those incurred in all historical wars [52]. Global tracking initiatives, including platforms like Worldometers and the Center for Systems Science and Engineering (CSSE) at Johns Hopkins University, have played a pivotal role in monitoring the virus's spread [27]. As COVID-19 swiftly spread worldwide, India experienced its impact as well. The nation confirmed its first locally transmitted case on January 30, 2020, in Kerala's Thrissur district, where a student returning from Wuhan University tested positive [22]. Concerns regarding insufficient testing rates raised alarms about potential widespread infections [9]. With a transmission rate of 1.7 [54], India's spread was comparatively lower than other global hotspots, though its estimated basic reproduction number (R_c) ranged from 2 to 3.5 [4, 63]. The high viral loads in the upper respiratory tract of symptomatic and asymptomatic individuals facilitated silent transmission, akin to influenza [63].

During the early phases of a pandemic, when healthcare resources and biomedical interventions are insufficient, public education on preventive measures becomes the most effective strategy for controlling disease spread. Non-pharmaceutical interventions (NPIs) such as social distancing, mask mandates, and quarantine protocols have been widely disseminated through social media, television, radio, and the internet [49, 48]. Modern research underscores the power of media coverage as a behavioral influence mechanism, capable of shaping public responses without direct economic investment [21]. Several studies have explored the role of media in mitigating infectious disease outbreaks [40, 12, 2, 42, 58, 15, 44]. Misra, Sharma, and Shukla [40] analyzed a nonlinear SIS model demonstrating that media-driven awareness campaigns can significantly reduce transmission by encouraging individuals to self-isolate. Chang et al. [12] examined the impact of media coverage during the COVID-19 outbreak in Hubei, China, finding that reduced media attention delayed the infection peak but ultimately increased overall case numbers. Aldila [2] approached media and rapid testing interventions as an optimal control problem, demonstrating their effectiveness in minimizing in-

fections and economic disruptions in East Java, Indonesia. In India, Rai et al. [42] assessed the influence of social media advertisements on COVID-19 transmission. Wang et al. [58] and Chen, Li, and Zhang [15] conducted sensitivity analyses showing that intensified media campaigns can reduce the adequate reproduction number and curb infection rates. The findings emphasize the necessity of NPIs in reducing the basic reproduction number below one. Regular public health campaigns and digital outreach efforts are essential in encouraging symptomatic individuals to seek hospitalization and asymptomatic carriers to enter quarantine, thereby mitigating viral spread. Media coverage significantly influences human behavior, prompting adherence to precautionary measures such as lockdowns [19, 31], social distancing [13, 18], mask usage [7, 37, 8], quarantine enforcement [7, 34, 1], and hospitalization protocols [47, 25]. Studies have demonstrated the effectiveness of NPIs in controlling COVID-19 transmission. Sardar et al. [45] evaluated lockdown measures across Indian states, revealing a decline in virus transmission. Aldila et al. [3] employed mathematical modeling to assess the impact of social distancing and rapid assessments in Jakarta, Indonesia. Memon, Qureshi, and Memon [39] examined the efficacy of quarantine and isolation in mitigating outbreaks. Srivastav et al. [50] analyzed the effects of face masks, hospitalization, and asymptomatic quarantine on disease transmission in India, concluding that these strategies significantly reduce infection rates. Additionally, Wang and Ruan [57] introduced an epidemic model incorporating constant removal of infectives through treatment, revealing complex transmission dynamics. Yuan et al. [61] proposed an $SEII_aHR$ model investigating the impact of asymptomatic carriers and isolation measures on global COVID-19 transmission.

While most studies focus on human-to-human transmission, SARS-CoV-2 also spreads through contaminated environments. Infected individuals introduce the virus into their surroundings via respiratory secretions from coughing or sneezing [23], and the virus can persist on surfaces for several days [56]. Several mathematical models have explored the role of environmental contamination in disease spread [53, 46, 5]. For instance, Sarkar, Mondal, and Khajanchi [46] assessed COVID-19 transmission in India, demonstrating that higher environmental contamination correlates with increased infection

rates. Asamoah et al. [5] conducted a similar study in Ghana, emphasizing the need for sanitation measures. These findings highlight the critical role of hygiene and disinfection practices in controlling the virus.

Motivated by the work of Asamoah et al. [5], this study develops a novel mathematical model to analyze COVID-19 transmission dynamics and evaluate intervention strategies in India. Rai et al. [42] illustrated how individuals adjust their behavior based on perceived susceptibility to infection. This research incorporates a saturation-type incidence function [41] to account for adaptive responses such as mask-wearing, hand hygiene, and social distancing. Using dynamical systems theory, numerical simulations, and sensitivity analyses, the study provides critical insights into the effectiveness of various control strategies. Model parameters are estimated using data from India collected between March 2020 and January 2021 [27]. Optimal control theory offers a robust mathematical framework for identifying the most effective strategies to manage infectious disease outbreaks. This approach has been widely utilized to design public health policies aimed at minimizing transmission [7, 5, 32, 62, 16, 20]. The present study applies optimal control theory to refine and evaluate the proposed model, ensuring its practical applicability in pandemic management.

The article is structured as follows: Section 2 presents the mathematical model describing COVID-19 transmission dynamics. In Section 3, the model's well-posedness is demonstrated, followed by an analysis of equilibrium points, stability assessment, and the control reproduction number evaluation. Section 4 is dedicated to numerical investigations, including parameter estimation based on empirical data, normalized sensitivity analysis, and simulations that examine the effects of NPIs and environmental contamination on the spread of the disease. Section 5 addresses the formulation and solution of the optimal control problem. Lastly, Section 6 concludes the study and outlines possible directions for future research.

2 Mathematical model

In this section, we introduce a novel mathematical model for COVID-19. The human population is categorized into eight groups: Susceptible indi-

viduals (S), exposed individuals (E), symptomatic infected individuals (I), asymptomatic infected individuals (I_a), aware individuals (A), and recovered individuals (R). Additionally, U represents the density of the coronavirus in the environment, while M denotes the media coverage of COVID-19, encompassing social media, print, electronic media, radio, and similar platforms. The model is based on the following assumptions:

1. The population's composition stays unchanged, as new individuals enter the region at a constant rate Λ and are immediately added to the susceptible group upon arrival.

2. Disease transmission occurs when a susceptible individual comes into contact with an infected individual, transitioning into the exposed category at a rate represented by β.

3. $1/\sigma$ represents the latent period. The exposed individuals who do not exhibit clinical symptoms join the asymptomatic infected class at a rate of $(1-\sigma)k_2$. In contrast, those who exhibit clinical symptoms join the symptomatic infected class at a rate of σk_1.

4. During an endemic outbreak, health authorities and media outlets leverage social media platforms such as Facebook, Twitter, and WhatsApp to share information with the public. The spread of information is influenced by both the frequency of its dissemination and the severity of the outbreak it pertains to. This suggests that the pace at which information campaigns grow is closely tied to the scale of the affected population [40].

5. Media coverage has a limited impact on how the disease spreads among susceptible individuals. As a result, the rate at which susceptible people become aware is modeled by $\frac{\lambda MS}{c+M}$, where c represents the half-saturation constant indicating the media exposure level at which awareness reaches half its maximum effect. When the level of media coverage reaches c, it reaches half its maximum value λS as in [41]. Even those in the aware class can lose their awareness and return to the susceptible class at the rate λ_0. Additionally, the region consistently receives a minimum level of media attention.

6. A proportion α of people in public places consistently and correctly wear face masks. When face masks are worn properly, they reduce the spread of disease [28].

7. Individuals showing symptoms move into the recovered class at the rate γ_3. Over time, immunity in the recovered group wanes, causing them to re-enter the susceptible group at a rate of ξ. Moreover, symptomatic infected individuals die due to the disease at a rate given by δ.

8. In the model, a fixed proportion ϕ of newly asymptomatic infections is assumed to progress to the symptomatic class, whereas the complementary fraction $1-\phi$ recovers without ever developing symptoms. Individuals in the ϕ-branch leave the asymptomatic compartment I_a at rate γ_1 (mean waiting time $1/\gamma_1$) and join the symptomatic class I; strictly asymptomatic cases exit I_a at rate γ_2 (mean infectious period $1/\gamma_2$) and enter the recovered class R [5].

   Asymptomatic individuals who do not display symptoms join the recovered class at the rate γ_2.

9. A person infected with COVID-19 releases the virus into the surroundings by sneezing or coughing. The emission rates of the virus by asymptomatic and symptomatic individuals are represented by θ_1 and θ_2, respectively. However, the virus does not persist indefinitely in the environment; it is gradually removed through natural decay and human efforts such as cleaning and disinfection. The rate at which the virus is eliminated from the surroundings is denoted by ϵ.

10. The rate of information growth, symbolized as r_1, is assumed to be directly linked to the number of infected individuals. The growth rate decreases by a factor of

$$f(A) = \frac{r_1 \theta A}{\omega + A}.$$

    Consequently, the net growth rate of TV and social media advertisements aimed at raising awareness within the population is expressed as

$$r_1 \left(1 - \frac{\theta A}{\omega + A}\right).$$

Here, θ represents the rate of decline in advertisement effectiveness as the number of aware individuals increases. The parameter ω denotes the half-saturation point, where $f(A)$ achieves half of its maximum value $r_1\theta$, occurring when the aware population reaches ω. For the model to remain valid, the value of θ must lie between 0 and 1. Meanwhile, the rate of information decay, indicated by r_0, quantifies how quickly memories of the information naturally diminish over time.

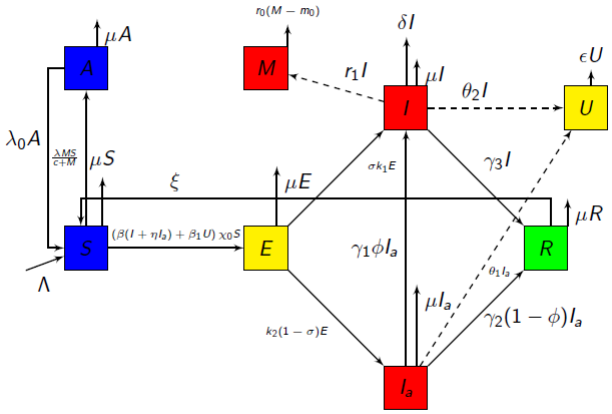

Figure 1: Flow diagram of model (1)

The spread of COVID-19, based on the stated assumptions, can be modeled using the following system of nonlinear ordinary differential equations:

$$\begin{cases} \frac{dS}{dt} &= \Lambda - \beta(1-\alpha)(I+\eta I_a)S - \beta_1(1-\alpha)SU + \lambda_0 A + \xi R - \frac{\lambda MS}{c+M} - \mu S, \\ \frac{dA}{dt} &= \frac{\lambda MS}{c+M} - \lambda_0 A - \mu A, \\ \frac{dE}{dt} &= \beta(1-\alpha)(I+\eta I_a)S + \beta_1(1-\alpha)SU - k_2(1-\sigma)E - k_1\sigma E - \mu E, \\ \frac{dI_a}{dt} &= k_2(1-\sigma)E - \gamma_1\phi I_a - \gamma_2(1-\phi)I_a - \mu I_a, \\ \frac{dI}{dt} &= k_1\sigma E + \gamma_1\phi I_a - \gamma_3 I - \delta I - \mu I, \\ \frac{dR}{dt} &= \gamma_2(1-\phi)I_a + \gamma_3 I - \xi R - \mu R, \\ \frac{dU}{dt} &= \theta_1 I_a + \theta_2 I - \epsilon U, \\ \frac{dM}{dt} &= r_1(1-\frac{\theta A}{\omega+A})I - r_0(M-m_0). \end{cases} \tag{1}$$

A flow diagram of the model (1) is depicted in Figure 1. The initial circumstances of model (1) are regarded as follows:
$S(0) = S_0 > 0, \quad E(0) \geq 0, \quad I_a(0) \geq 0, \quad I(0) \geq 0, \quad A(0) = A_0 \geq 0, \quad R(0) \geq 0, \quad U(0) \geq 0, \quad M(0) \geq m_0.$

Let us use the notations: $\chi_0 = (1-\alpha), \quad \chi_1 = k_2(1-\sigma) + k_1\sigma + \mu, \quad \chi_2 = \gamma_1\phi + \gamma_2(1-\phi) + \mu, \quad \chi_3 = \gamma_3 + \delta + \mu, \quad \chi_4 = \lambda_0 + \mu, \quad \chi_5 = \xi + \mu.$

Consequently, the above model (1) can be expressed as

$$\begin{cases} \frac{dS}{dt} &= \Lambda - \beta\chi_0(I + \eta I_a)S - \beta_1\chi_0 SU + \lambda_0 A + \xi R - \frac{\lambda MS}{c+M} - \mu S, \\ \frac{dA}{dt} &= \frac{\lambda MS}{c+M} - \chi_4 A, \\ \frac{dE}{dt} &= \beta\chi_0(I + \eta I_a)S + \beta_1\chi_0 SU - \chi_1 E, \\ \frac{dI_a}{dt} &= k_2(1-\sigma)E - \chi_2 I_a, \\ \frac{dI}{dt} &= k_1\sigma E + \gamma_1\phi I_a - \chi_3 I, \\ \frac{dR}{dt} &= \gamma_2(1-\phi)I_a + \gamma_3 I - \chi_5 R, \\ \frac{dU}{dt} &= \theta_1 I_a + \theta_2 I - \epsilon U, \\ \frac{dM}{dt} &= r_1(1 - \frac{\theta A}{\omega + A})I - r_0(M - m_0). \end{cases} \tag{2}$$

A description of all parameters is given in Table 1.

3 Mathematical analysis

In this section, we provide essential analytical findings for model (1), demonstrating that its solutions remain positive and bounded. We also identify disease-free and endemic equilibrium states and examine their stability. In addition, we derive a theoretical expression for the critical biological parameter known as the control reproduction number.

Table 1: Parameters and their interpretation for models (1)

Parameters	Description
η	Modification Parameter for asymptomatic class
β	Human-to-human transmission rate
β_1	Maximum transmission rate due to environmental contamination
k_1	Progression rate from exposed to the symptomatic class
k_2	Progression rate from exposed to the asymptomatic class
γ_3	Recovery rate for symptomatic infected individuals
λ	The rate at which awareness spreads among susceptible individuals
c, ω	Half saturation constants
γ_1	Rate of transition from asymptomatic to symptomatic class
γ_2	Rate of transition from asymptomatic to recovered class
δ	Disease-induced mortality rate for symptomatic individuals
ϕ	The fraction of asymptomatic patients who subsequently develop symptoms and transition to the symptomatic infected class
Λ	Recruitment rate
r_1	Development rate of information dissemination
r_0	Reduction rate of advertisements due to inefficacy and psychological barriers
μ	Natural death rate
m_0	Baseline number of media coverage
λ_0	Rate of transition of aware individuals to the susceptible class
α	The proportion of the population wearing face masks
θ_1	The speed at which asymptomatic individuals emit the virus into their surroundings
θ_2	The rate at which symptomatic individuals emit the virus into their surroundings
ϵ	Natural decay rate of virus from the environment
θ	Represent the decline in the effectiveness of advertisements as the number of individuals who are already aware increases
$1/\xi$	Average time it takes for immunity to wear off
σ	Fraction of exposed individuals joint to I class

3.1 Positivity and boundedness

In this section, we demonstrate that the solutions of the model (1) are positive and bounded.

$$\left.\frac{dS}{dt}\right|_{S=0} = \Lambda + \lambda_0 A + \xi R > 0, \qquad \left.\frac{dA}{dt}\right|_{A=0} = \frac{\lambda M S}{c+M} \geq 0,$$
$$\left.\frac{dI_a}{dt}\right|_{I_a=0} = k_2(1-\sigma)E \geq 0, \qquad \left.\frac{dI}{dt}\right|_{I=0} = k_1\sigma E + \gamma_1\phi I_a \geq 0,$$
$$\left.\frac{dE}{dt}\right|_{E=0} = \beta\chi_0(I+\eta I_a)S + \beta_1\chi_0 SU \geq 0, \quad \left.\frac{dR}{dt}\right|_{R=0} = \gamma_3 I + \gamma_2(1-\phi)I_a > 0,$$
$$\left.\frac{dU}{dt}\right|_{U=0} = \theta_2 I + \theta_1 I_a \geq 0, \qquad \left.\frac{dM}{dt}\right|_{M=0} = r_1 I + r_0 m_0 > 0.$$

As all rates are nonnegative in this scenario, any solution starting within the interior of the nonnegative bounding cone $\mathbb{R}^8_+$ will remain confined to this cone, as the vector field consistently points inward along all bounding planes. As a result, it is assured that none of the model (1) solutions are negative. We add equations of the model (1) to demonstrate the boundedness of its solutions, which results in $\frac{dN}{dt} = \Lambda - \mu N - \delta I$. Then, $\frac{dN}{dt} < \Lambda - \mu N$, Applying Birkhoff's and Rota's theorems on differential inequality [10], as $t \to \infty$, we have $0 \leq N(t) \leq \frac{\Lambda}{\mu}(= N_0)$. As $I(t), I_a(t) \leq N(t)$ at any time, so $I(t), I_a(t) \leq \frac{\Lambda}{\mu}$. Now, from the density of the virus in the environment, $\frac{dU}{dt} = \theta_2 I + \theta_1 I_a - \epsilon U \leq (\theta_2 + \theta_1)\frac{\Lambda}{\mu} - \epsilon U$. For the initial conditions, when applying the Gronwall inequality, we get $0 \leq U(0) \leq \frac{(\theta_2+\theta_1)\Lambda}{\epsilon\mu}$. Additionally, from the eighth equation of model (1), we obtain $\frac{dM}{dt} + r_0 M \leq r_0 m_0 + \frac{r_1\Lambda}{\mu}$. Using differential inequality theory, we can derive

$$\limsup M(t) \leq m_0 + \frac{r_1\Lambda}{r_0\mu},$$

when applying the Gronwall inequality $0 \leq M(0) \leq m_0 + \frac{r_1\Lambda}{r_0\mu}$. Hence, the feasible region for the model (1) is

$$\Theta = \left\{ (S, A, E, I_a, I, R, U, M) \in \mathbb{R}^8_+ : \right.$$
$$\left. 0 \leq S, A, E, I_a, I, R, N \leq \frac{\Lambda}{\mu}; \right.$$

$$0 \leq U \leq \frac{(\theta_2+\theta_1)\,\Lambda}{\epsilon\mu}; 0 < M \leq m_0 + \frac{r_1\Lambda}{r_0\mu}\Bigg\}. \tag{3}$$

Therefore, Θ defines the region enclosing the model's solutions.

Theorem 1. Solutions of the model under the given initial conditions continue to be nonnegative as time goes on. Furthermore, the closed region remains unchanged and preserved under the dynamics of the model (1).

3.2 Disease-free equilibrium (DFE) and basic reproduction number

The disease-free equilibrium (DFE) of the model (1) is given by $\zeta_0 = (S_0, A_0, 0, 0, 0, 0, 0, m_0)$, where $S_0 = \frac{(c+m_0)\Lambda(\lambda_0+\mu)}{\mu(m_0\lambda+c\lambda_0+m_0\lambda_0+c\mu+m_0\mu)}$ and $A_0 = \frac{m_0\Lambda\lambda}{\mu(m_0\lambda+c\lambda_0+m_0\lambda_0+c\mu+m_0\mu)}$.

The control reproduction number for model (2) is determined using the following generation matrix approach [55]. By defining the state vector as $x = (E, I_a, I, U)$, the system in model (2) can be reformulated as $\frac{dx}{dt} = \mathcal{F}(x) - \mathcal{V}(x)$, where $\mathcal{F}$ represents the nonnegative matrix of new infection terms, and the matrix $\mathcal{V}$ of the remaining terms are given by

$$\mathcal{F} = \begin{bmatrix} \beta\chi_0(I+\eta I_a)S + \beta_1\chi_0 SU \\ 0 \\ 0 \\ 0 \end{bmatrix}, \mathcal{V} = \begin{bmatrix} \chi_1 E \\ -k_2(1-\sigma)E + \chi_2 I_a \\ -k_1\sigma E - \gamma_1\phi I_a + \chi_3 I \\ -\theta_1 I_a - \theta_2 I + \epsilon U \end{bmatrix}.$$

The corresponding linearized matrices evaluated at the DFE ζ_0 are

$$F_1 = \begin{bmatrix} 0 & S_0\chi_0\beta\eta & S_0\chi_0\beta & S_0\chi_0\beta_1 \\ 0 & 0 & 0 & 0 \\ 0 & 0 & 0 & 0 \\ 0 & 0 & 0 & 0 \end{bmatrix}, V_1 = \begin{bmatrix} \chi_1 & 0 & 0 & 0 \\ -k_2(1-\sigma) & \chi_2 & 0 & 0 \\ -k_1\sigma & -\gamma_1\phi & \chi_3 & 0 \\ 0 & -\theta_1 & -\theta_2 & \epsilon \end{bmatrix}.$$

We get control reproduction number $R_c = \rho\left(F_1 V_1^{-1}\right)$, where ρ is the spectral radius.

$R_c = \frac{S_0\chi_0(k_1(\beta\epsilon+\beta_1\theta_2)\phi\chi_2+k_2(1-\phi)(\beta\epsilon(\eta\chi_3+\gamma_1\phi)+\beta_1(\theta_1\chi_3+\gamma_1\theta_2\phi)))}{\epsilon\chi_1\chi_2\chi_3}$.

In the absence of any intervention and behavioral awareness, $\alpha = 0, \lambda = 0, \lambda_0 = 0,\ m_0 = 0$, implies $A_0 = 0, S_0 = \frac{\Lambda}{\mu} = N_0$. Hence, the basic reproduction number R_0 of the model (2) is given by $R_0 = \frac{N_0\left[k_1\left(\beta\epsilon+\beta_1\theta_2\right)\phi\,\chi_2 + k_2(1-\phi)\left(\beta\epsilon\left(\eta\chi_3+\gamma_1\phi\right)+\beta_1\left(\theta_1\chi_3+\gamma_1\theta_2\phi\right)\right)\right]}{\epsilon\,\chi_1\chi_2\chi_3}$. It is clear that $R_c = \frac{S_0\chi_0 R_0}{N_0}$. Since $\frac{S_0}{N_0} \leq 1$ and $0 \leq \chi_0 \leq 1$, this implies that $R_c \leq R_0$.

Theorem 2. The equilibrium state ζ_0, representing the absence of disease in the model (2), remains locally asymptotically stable provided that the control reproduction number R_c is less than one. Conversely, it loses stability when R_c exceeds one.

3.3 Global stability

This section examines the global stability of the disease-free steady state for a specific case.

Theorem 3. The DFE ζ_0 in model (2) is globally asymptotically stable when $R_c \leq 1$; however, it becomes unstable if $R_c > 1$.

Proof. We construct a suitably defined Lyapunov function to establish the global stability of the DFE ζ_0. Specifically, we consider a continuously differentiable, positive definite function $\mathcal{G}$ such that

$$\mathcal{G} = d_1E + d_2I_a + d_3I + d_4U. \tag{4}$$

The constants $d_j \geq 0$ for $j = 1, 2, \ldots, 4$ will be determined later. Furthermore, by utilizing the equations from model (1) and differentiating equation (4), we obtain

$$\begin{aligned}
\mathcal{G}' =& d_1E' + d_2I_a' + d_3I' + d_4U' \\
=& d_1(\beta\chi_0(I+\eta I_a)S + \beta_1\chi_0 SU - \chi_1 E) + d_2(k_2(1-\sigma)E - \chi_2 I_a) \\
&+ d_4(\theta_1 I_a + \theta_2 I - \epsilon U) + d_3(k_1\sigma E + \gamma_1\phi I_a - \chi_3 I) \\
\leq& d_1(\beta\chi_0(I+\eta I_a)S_0 + \beta_1\chi_0 S_0 U - \chi_1 E) + d_2(k_2(1-\sigma)E - \chi_2 I_a) \\
&+ d_4(\theta_1 I_a + \theta_2 I - \epsilon U) + d_3(k_1\sigma E + \gamma_1\phi I_a - \chi_3 I) \\
=& \left(-\chi_1 d_1 + d_2k_2(1-\sigma) + d_3k_1\sigma\right)E + \left(d_1\beta\eta\chi_0 S_0 - d_2\chi_2 + d_3\gamma_1\phi + d_4\theta_1\right)I_a
\end{aligned}$$

$$+ \left(d_1\beta\chi_0 S_0 - d_3\chi_3 + d_4\theta_2\right) I + \left(d_1\chi_0\beta_1 S_0 - d_4\epsilon\right) U. \tag{5}$$

Let us choose the constant values as follows: $d_4 = 1, d_3 = \frac{(\beta\epsilon+\beta_1\theta_2)}{\beta_1\chi_3}, d_1 = \frac{\epsilon}{\chi_0 S_0\beta_1}, d_2 = \frac{\beta\epsilon\eta\chi_3+\beta_1\theta_1\chi_3+\beta\gamma_1\epsilon\phi+\beta_1\gamma_1\theta_2\phi}{\beta_1\chi_2\chi_3}$, using the aforementioned inequality (5), we obtain the following:

$$\mathcal{G}' \leq \frac{(R_c - 1)\chi_1\epsilon E}{S_0\beta_1\chi_0}. \tag{6}$$

Clearly, $\mathcal{G}' \leq 0$ whenever $R_c \leq 1$, and $\mathcal{G}' = 0$ if and only if either $E = 0$ or $R_c = 1$, at DFE. Therefore, by LaSalle's invariance principle [35], the equilibrium point ζ_0 is globally asymptotically stable. □

3.4 Presence and persistence of endemic equilibria

To determine the possible endemic equilibrium points of the proposed model, the system of nonlinear equations derived from the model (2) is solved by setting all derivatives to zero. The endemic equilibrium $\zeta^* = \{S^*, A^*, E^*, I_a^*, I^*, R^*, U^*, M^*\}$, of the model (2) is given by

$$E^* = b_1 I_a^*, I^* = b_2 I_a^*, A^* = \frac{b_5 M^*\lambda}{(M^* + c)\chi_4}, R^* = b_3 I_a^*, U^* = b_4 I_a^*,$$

$$M^* = b_1 I^* + m_0, S^* = b_5.$$

Putting the values of $\{S^*, A^*, E^*, I^*, R^*, U^*\}$ in the first, second, and eighth equation of system of equations (1), we have

$$\Lambda + b_3\xi I_a^* + b_5\left(-\mu - (b_4\beta_1 + \beta(b_2 + \eta))\chi_0 I_a^* + \frac{\lambda(\lambda_0 - \chi_4)M^*}{(M^* + c)\chi_4}\right) = 0, \tag{7}$$

$$m_0 r_0 + b_2 r_1 I_a^* = \left(r_0 + \frac{b_2 b_5 r_1\theta\lambda I_a^*}{b_5\lambda M^* + (M^* + c)\chi_4\omega}\right) M^*, \tag{8}$$

where

$$b_1 = \frac{\chi_2}{k_2(1-\phi)}, \quad b_2 = \frac{b_1 k_1\phi + \gamma_1\phi}{\chi_3}, \quad b_3 = \frac{\gamma_2(1-\phi) + b_2\gamma_3}{\chi_5},$$

$$b_4 = \frac{\theta_1 + b_2\theta_2}{\epsilon}, b_5 = \frac{b_1\chi_1}{\chi_0(b_4\beta_1 + \beta(b_2 + \eta))}.$$

Equations (7) and (8) represent two isoclines in I_a^* and M^*. Analyzing the behavior of these isoclines through mathematical methods is challenging. Let (I_a^*, M^*) denote the unique point where these isoclines intersect.

We have seen that at least one endemic equilibrium always exists. Additionally, we investigate the occurrence of transcritical bifurcation through the application of center manifold theory, as detailed in previous studies [11, 43]. To simplify the process, we modify the variables accordingly and employ a similar approach described in those references [11]:
$S = x_1 + S_0, \quad E = x_2, \quad I_a = x_3, \quad I = x_4, \quad A = x_5 + A_0, \quad R = x_6, \quad U = x_7, \quad M = x_8 + m_0$. As a result, it is possible to rewrite model (1) compactly, as follows:

$$\begin{cases} \frac{dx_1}{dt} & = \Lambda - \chi_0\beta(x_4 + \eta x_3)(x_1 + S_0) - \beta_1\chi_0(x_1 + S_0)x_7 + \xi x_6) \\ & \quad +\lambda_0(x_5 + A_0 - \frac{\lambda(x_8+m_0)(x_1+S_0)}{c+(x_8+m_0)} - \mu(x_1 + S_0), \\ \frac{dx_2}{dt} & = \beta\chi_0(x_4 + \eta x_3)(x_1 + S_0) + \beta_1\chi_0(x_1 + S_0)x_7 - \chi_1 x_2, \\ \frac{dx_3}{dt} & = k_2(1 - \sigma)x_2 - \chi_2 x_3, \\ \frac{dx_4}{dt} & = k_1\sigma x_2 + \gamma_1\phi x_3 - \chi_3 x_4, \\ \frac{dx_5}{dt} & = \frac{\lambda(x_8+m_0)(x_1+S_0)}{c+(x_8+m_0)} - \chi_5(x_5 + A_0), \\ \frac{dx_6}{dt} & = \gamma_2(1 - \phi)x_3 + \gamma_3 x_4 - \chi_6 x_6, \\ \frac{dx_9}{dt} & = \theta_1 x_3 + \theta_2 x_4 - \epsilon x_7, \\ \frac{dx_{10}}{dt} & = r_1\left(1 - \frac{\theta(x_5+A_0)}{\omega+(x_5+A_0)}\right)x_4 - r_0 x_8. \end{cases} \tag{9}$$

The Jacobian matrix of model (9) at the corresponding DFE P^0 is given by

$$J_{P^0} = \begin{bmatrix} -c_2 & 0 & -S_0\beta_c\eta\chi_0 & -S_0\beta_c\chi_0 & \lambda_0 & \xi & -S_0\beta_1\chi_0 & c_4 \\ 0 & -\chi_1 & s_0\beta_c\eta\chi_0 & S_0\beta_c\chi_0 & 0 & 0 & s_0\beta_1\chi_0 & 0 \\ 0 & k_2(1-\phi) & -\chi_2 & 0 & 0 & 0 & 0 & 0 \\ 0 & k_1\phi & \gamma_1\phi & -\chi_3 & 0 & 0 & 0 & 0 \\ c_1 & 0 & 0 & 0 & -\chi_4 & 0 & 0 & -c_4 \\ 0 & 0 & \gamma_2(1-\phi) & \gamma_3 & 0 & -\chi_5 & 0 & 0 \\ 0 & 0 & \theta_1 & \theta_2 & 0 & 0 & -\epsilon & 0 \\ 0 & 0 & 0 & c_3 & 0 & 0 & 0 & -r_0 \end{bmatrix},$$

where

$c_1 = \frac{\lambda m0}{c+m0}, c_2 = \mu + c_1, c_3 = r_1\left(1 - \frac{\theta A_0}{\omega + A_0}\right), c_4 = -\frac{cS_0\lambda}{(c+m_0)^2}, c_5 = -c_4.$

At $R_c = 1$, the bifurcation parameter β gives a critical β_c as

$$\beta_c = \frac{-k_1S_0\beta_1\theta_2\phi\chi_0\chi_2 + \epsilon\chi_1\chi_2\chi_3 - k_2S_0\beta_1(1-\phi)\chi_0(\theta_1\chi_3 + \gamma_1\theta_2\phi)}{S_0\epsilon\chi_0(k_1\phi\chi_2 + k_2(1-\phi)(\eta\chi_3 + \gamma_1\phi))}.$$

Confirming that the Jacobian evaluated at $\beta = \beta_c$ possesses a right eigenvector associated with the zero eigenvalue is

$\mathbf{W} = (w_1, w_2, w_3, w_4, w_5, w_6, w_7, w_8)^T$, where $w_2 = 1, \quad w_3 = a_1, w_4 = a_2,$

$w_7 = a_4, \quad w_6 = a_5, \quad w_8 = a_3,$

$w_1 = -\frac{-a_3c_4\lambda_0 + a_3c_4\chi_4 + a_5\xi\chi_4 - a_4s_0\beta_1\chi_0\chi_4 - a_2s_0\beta_c\chi_0\chi_4 - a_1s_0\beta_c\eta\chi_0\chi_4}{c_1\lambda_0 - c_2\chi_4},$

$w_5 = -\frac{-a_3c_1c_4 + a_3c_2c_4 - a_5c_1\xi + a_4c_1s_0\beta_1\chi_0 + a_2c_1s_0\beta_c\chi_0 + a_1c_1s_0\beta_c\eta\chi_0}{-c_1\lambda_0 + c_2\chi_4},$

where $a_1 = \frac{k_2(1-\phi)}{\chi_2}, a_2 = \frac{k_1\phi + a_1\gamma_1\phi}{\chi_3}, \quad a_3 = \frac{a_2c_3}{r_0}, \quad a_4 = \frac{a_1\theta_1 + a_3\theta_2}{\epsilon}, \quad a_5 = \frac{a_1\gamma_2(1-\phi) + a_3\gamma_3}{\chi_5}.$

The elements of the left eigenvector, which correspond to the zero eigenvalues, are also $\mathbf{V} = (v_1, v_2, v_3, v_4, v_5, v_6, v_7, v_8)$ and must satisfy the equalities $V.J = 0$ and $V.W = 1$, so that we obtain

$v_1 = 0, \quad v_5 = 0, \quad v_6 = 0, \quad v_8 = 0, \quad v_3 = \frac{k_1S_0v_2\beta_c\epsilon\phi\chi_0 + k_1S_0v_2\beta_1\theta_2\phi\chi_0 - v_2\epsilon\chi_1\chi_3}{k_2\epsilon(-1+\phi)\chi_3},$

$v_4 = \frac{S_0v_2\beta_c\epsilon\chi_0 + S_0v_2\beta_1\theta_2\chi_0}{\epsilon\chi_3}, \quad v_7 = \frac{s_0v_2\beta_1\chi_0}{\epsilon},$

$v_2 = \frac{k_2\epsilon(-1+\phi)\chi_3}{a_2k_2S_0(\beta_c\epsilon + \beta_1\theta_2)(-1+\phi)\chi_0 + a_1k_1S_0(\beta_c\epsilon + \beta_1\theta_2)\phi\chi_0 + k_2(-1+\phi)(\epsilon + a_4S_0\beta_1\chi_0)\chi_3 - a_1\epsilon\chi_1\chi_3}.$

As outlined in [11, Theorem 4.1], the bifurcation coefficients a and b can be determined using the following expressions, where f_k represents the k^{th} component of the vector function f:

$$
\begin{aligned}
a &= \sum_{k,i,j=1}^{10} v_k w_i w_j \frac{\partial^2 f_k}{\partial x_i \partial x_j}(0,0) \\
&= v_2 \left(2w_1 w_7 \beta_1 \chi_0 + 2w_1 w_4 \beta_c \chi_0 + 2w_1 w_3 \beta_c \eta \chi_0\right), \\
b &= \sum_{k,i,j=1}^{10} v_k w_i \frac{\partial^2 f_k}{\partial x_i \partial \beta}(0,0) \\
&= S_0 w_4 \chi_0 + S_0 w_3 \eta \chi_0. \qquad (10)
\end{aligned}
$$

If $a < 0$ and $b > 0$ at $\beta = \beta_c$, then according to [11, Theorem 4.1 and Remark 1], a transcritical bifurcation occurs at $R_c = 1$. Moreover, when $R_c > 1$, the unique endemic equilibrium remains locally asymptotically stable.

4 Numerical simulation

4.1 Parameter estimation

In this section, the proposed model is calibrated against observed data to evaluate its accuracy and predictive capabilities, offering valuable insights into the pandemic's progression and supporting effective response strategies. Initially, baseline values for the model parameters are established using COVID-19 data, relevant information, and published literature. Specifically, data on the total number of COVID-19 cases in India from March 30, 2020, to January 24, 2021, were considered [27]. The least squares method is used to align the observed data points, Y_i, with the estimated values, X_i, by minimizing the total squared differences between the observed values and the predicted curve [38]. This process involves minimizing the *sum of squared errors (SSE)*, expressed as

$$SSE = \sum_{i=1}^{n} (Y_i - X_i)^2$$

Table 2 and Figure 3 present the fitted model developed using MATLAB, along with the estimated parameter values. In Figure 3, the curve represents the fitted model, while the star points indicate the total number of daily confirmed cases. The estimated reproduction number (R_c) is 1.94, suggesting

a moderate transmission rate. The model simulation closely follows the actual data, demonstrating its reliability. Table 2 provides a detailed summary of the estimated and fitted parameters. Following this parameter estimation, we explore hypothetical scenarios where individuals neither wear masks nor are aware of COVID-19. A more in-depth discussion follows below.

Figure 2a illustrates the model's evaluation of India's response to COVID-19. Many disregarded safety measures during the prolonged lockdown and economic crisis, resulting in $\alpha = 0$ in Figure 2a. However, public awareness of COVID-19 remained high, leading to precautionary behaviors such as wearing face masks and self-quarantining after traveling from high-risk or red-alert zones. Figure 2b provides an alternative perspective, showing that even in cases where individuals were unaware of COVID-19's severity, many still adhered to protective measures like mask-wearing (i.e., $A = 0$ in 2b within 1). As illustrated in Figure 3, the model's predictions align closely with the observed data on daily new cases, reinforcing its applicability in understanding the pandemic's progression.

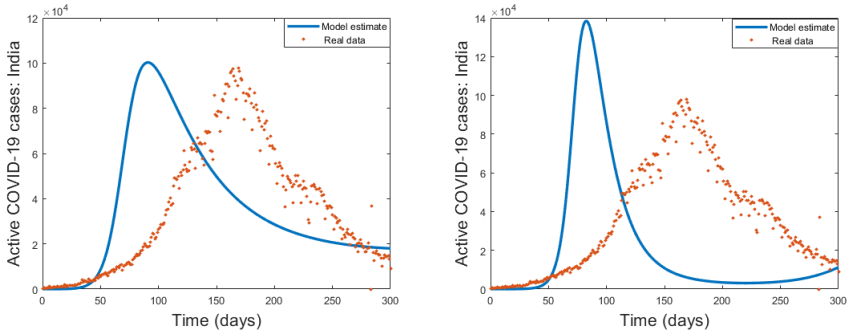

(a) $\alpha = 0$ only in (1) (b) $A = 0$ only in (1)

Figure 2: Fitted curve of confirmed cases in India and proposed model

4.2 Sensitivity analysis

Examining the sensitivity of parameters in the control reproduction number, R_c, is essential for understanding the dynamics of infectious diseases. This

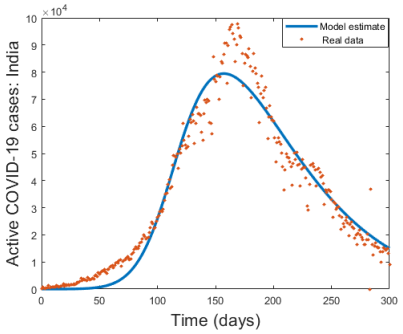

Figure 3: Fitted curve of confirmed case in India and model (1)

process enables the rapid identification of critical factors that drive disease transmission, which is pivotal for designing effective interventions. Modifying these parameters allows for more efficient pandemic management. The normalized forward sensitivity index of R_c with respect to a parameter p is defined as $\Gamma^p_{R_c} = \frac{\partial R_c}{\partial p}\frac{p}{R_c}$ [38, 24].

The sensitivity indices of R_c, derived using parameter values from Table 2, are presented in Table 3. It shows that R_c increases with increase in the values of $\Lambda, \beta, \beta_1, \sigma, \lambda_0, c, \theta_1, \theta_2, \eta, k_1, \gamma_1$, and ϕ. Conversely, parameters $m_0, \lambda, \epsilon, \delta, k_2$
$, \gamma_3, \gamma_2, \alpha$, and μ, have negative impact on R_c. Figure 4 indicates that Λ (λ) has the maximum positive (negative) impact on R_c. Lower R_c values are preferred for disease control. Reducing R_c to control disease transmission requires increasing control parameters with negative indices and decreasing those with positive indices. Furthermore, it can be seen that R_c is not affected by the model parameters $\xi, r_1, r_0, \omega, \theta$, that is,

$$\Gamma^{\xi}_{R_c} = \Gamma^{r_1}_{R_c} = \Gamma^{r_0}_{R_c} = \Gamma^{\omega}_{R_c} = \Gamma^{\theta}_{R_c} = 0.$$

Figure 5a displays a two-dimensional contour plot, while Figure 5b displays a three-dimensional contour plot of $R_c(\lambda, \lambda_0)$. Figure 5 demonstrates that as awareness rates increase over time, there is a substantial reduction in the incidence of COVID-19.

Table 2: Parameter values for the model (1)

Parameters	Range	Baseline	Source
η	$(0.6281, 0.6366)\ day^{-1}$	0.6364	[5]
β	$\left(6.038 \cdot 10^{-8}, 6.988 \cdot 10^{-8}\right)\ day^{-1}$	$6.933 \cdot 10^{-8}$	Estimated
β_1	$\left(3.00199 \cdot 10^{-8}, 4.10199 \cdot 10^{-8}\right)\ day^{-1}$	$4.00199 \cdot 10^{-8}$	[46]
k_1	$(0.0623, 0.0745)\ day^{-1}$	0.0723	Estimated
k_2	$(0.066, 0.08)\ day^{-1}$	0.068	Estimated
σ	$(0.065, 0.077)\ day^{-1}$	0.0749	Estimated
γ_1	$(0.15, 0.25)\ day^{-1}$	0.2	[5]
γ_2	$(0.159, 0.46)\ day^{-1}$	0.4599	Estimated
γ_3	$(0.018, 0.0668)\ day^{-1}$	0.066	Estimated
λ	$(0.0011, 0.0187)\ day^{-1}$	0.0186	[41]
λ_0	$(0.00001, 0.008)\ day^{-1}$	0.001	[41]
c	$(400, 2000)\ day^{-1}$	430	Estimated
δ	$(0.0066, 0.01)\ day^{-1}$	0.0099	[5]
ϕ	$(0.006999, 0.0099)\ day^{-1}$	0.00900005	Estimated
Λ	$(100, 3000)\ day^{-1}$	1319.294	[5]
r_1	$(0.001, 0.01)\ day^{-1}$	0.006	[41]
r_0	$(0.001, 0.01)\ day^{-1}$	0.005	[41]
μ	$(0.00001, 0.0001)\ day^{-1}$	0.0000425	[50]
m_0	$(100, 2000)\ day^{-1}$	500	[41]
θ_1	$(0.0158, 0.0178)\ day^{-1}$	0.0178	[5]
θ_2	$(0.1215, 9315)\ day^{-1}$	0.9215	[5]
ϵ	$(0.1, 0.2)\ day^{-1}$	0.333	[5]
θ	$(0.01, 0.034)\ day^{-1}$	0.0005	[41]
ξ	$(0.009, 0.01)\ day^{-1}$	0.008	Assumed
α	$(0.1, 0.2)\ day^{-1}$	0.3	Estimated
ω	$(0, 10000)\ day^{-1}$	6000	Estimated

4.3 Impact of control parameters

Figure 6a demonstrates that as awareness spreads more effectively, the number of symptomatic infections decreases, mainly because media coverage attracts susceptible people's attention. The rate at which people lose awareness, represented by λ_0, increases symptomatic infections, so efforts should be made to prevent this loss of awareness (see Figure 6b). To keep infection

Table 3: Normalized sensitivity index for each parameter for the COVID-19 model (1), for parameters values given in 2

Parameter	Sensitivity indices	Parameter	Sensitivity indices	Parameter	Sensitivity indices
Λ	1	η	0.65	γ_3	-0.26
β	0.76	σ	0.24	δ	-0.03
β_1	0.23	ϕ	0.07	α	-0.20
k_1	0.22	γ_1	0.06	k_2	-0.22
θ_1	0.03	ϵ	-0.23		
θ_2	0.19			λ	-0.88
λ_0	0.55	m_0	-0.25	μ	-0.55
c	0.25	γ_2	-0.75		

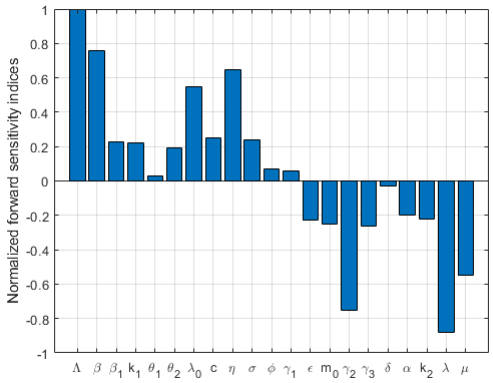

Figure 4: Normalized forward sensitivity indices of R_c

levels low, it is crucial to maintain a steady level of baseline awareness, m_0. Finally, to reduce the transmission rates β and β_1, measures like wearing masks, and so on (refer to Figure 7b) should be taken.

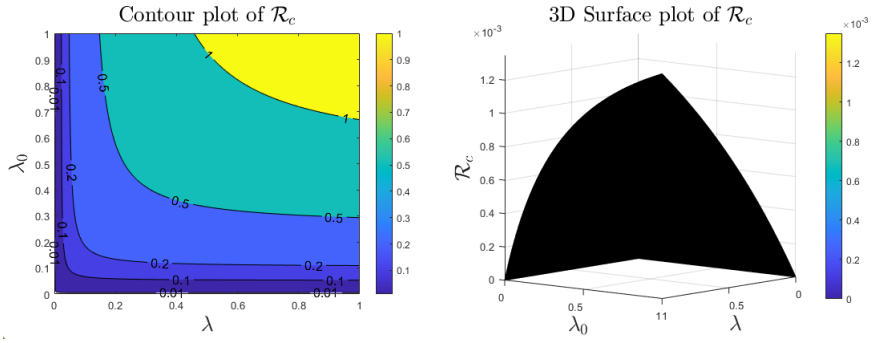

(a) $2D$ plot of $R_c(\lambda, \lambda_0)$ (b) 3-D contour of $R_c(\lambda, \lambda_0)$

Figure 5: contour plots of R_c

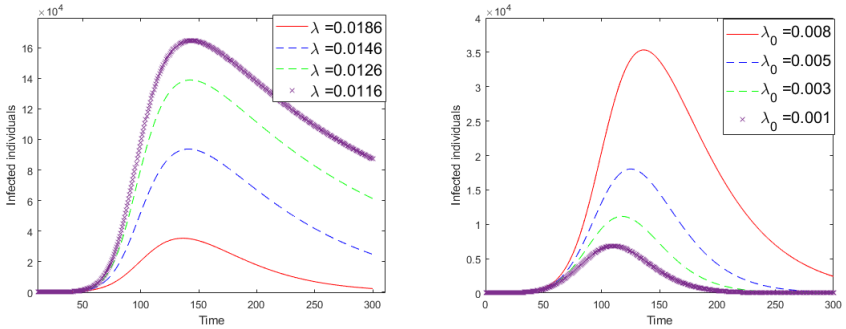

(a) Effect of λ on I (b) Effect of λ_0 on I

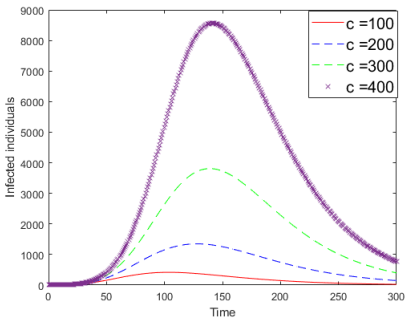

(c) Effect of c on I

Figure 6: The effects of varying λ, λ_0 and c on I.

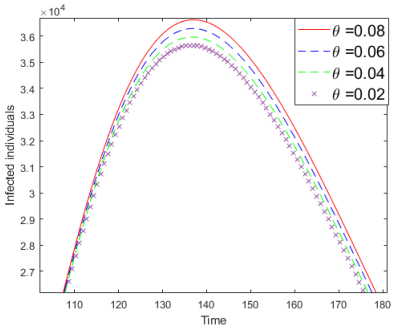

(a) Effect of θ on I

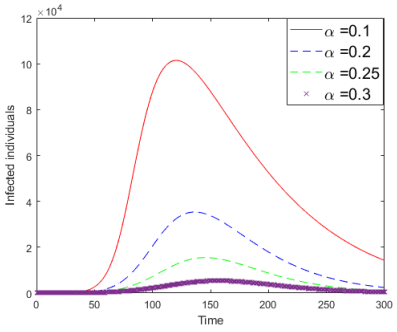

(b) Effect of α on I

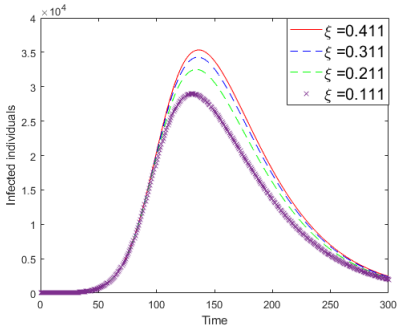

(c) Effect of ξ on I

Figure 7: The effects of varying θ, α and ξ on I.

4.4 Impact of environment contamination

Environmental contamination plays a significant role in the transmission of COVID-19. Studies show that the virus can remain viable on copper surfaces for up to four hours, on cardboard for as long as 24 hours, and on stainless steel and plastic surfaces for up to 72 hours [56]. This study examines how environmental contamination affects the dynamics of the proposed model, specifically analyzing the model (1) to assess the impact of COVID-19 on environmental contamination caused by infected individuals. The time series presented in Figures 8a, 8b, and 8c demonstrate the effects of environmental contamination parameters on infection levels.

The number of infected individuals in the class I increases as the infection rate β_1, associated with the contaminated environment increases. Furthermore, as the rate of environmental contamination (θ_1 and θ_2) increases, the populations in class I also grow, as shown in the time series Figures (8a and 8b). Consequently, an increase in the factors θ_1 and θ_2 results in a shorter duration of the pandemic. If the contaminated environment is sanitized effectively (i.e., by increasing ϵ), the number of infected individuals in class I_a and I remains relatively stable, as demonstrated in Figure 8c. Consequently, eliminating the novel coronavirus from environments can help shorten the pandemic's duration and lower infection rates.

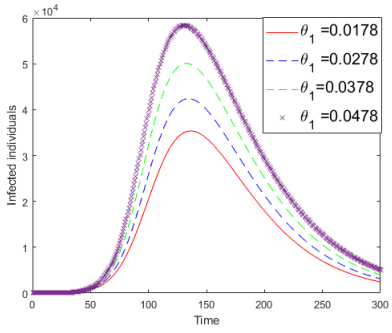

(a) Effect of θ_1 on I

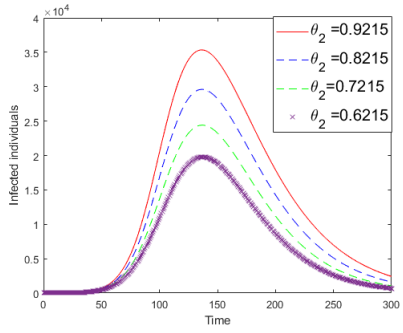

(b) Effect of θ_2 on I

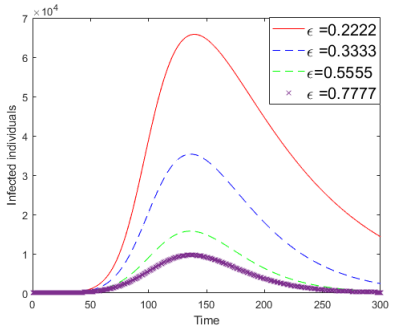

(c) Effect of ϵ on I

Figure 8: The effects of varying $\theta_1, \theta_2, \epsilon$ on infected population I.

5 Optimal Control

In this section, we develop and evaluate an optimal control problem that integrates multiple strategies, including the proportion of individuals using face masks, the level of awareness, treatment rates, and the natural decline of the virus in the environment. These measures aim to mitigate the spread of the disease while accounting for economic consequences, such as productivity losses caused by both the disease and the interventions. The subsequent discussion focuses on these control strategies:

1. Control variable $u_1(t)$: The susceptible population is continuously exposed to a proportion of individuals wearing face masks, represented by the rate α. Since implementing mask-wearing incurs costs, optimizing these costs is essential for policymakers. To achieve this, the mask-wearing rate α is treated as a control variable, $u_1(t)$, in the context of model (1), to determine the optimal intervention strategy.

2. Control variable $u_2(t)$: As information about the virus disseminates, susceptible individuals transition to an aware class, with the speed of this transition being affected by the concentration of the infected population. Since promoting awareness incurs certain costs, policymakers should aim to optimize these initiatives. Therefore, the awareness rate, denoted by λ, is modeled as a control variable $u_2(t)$.

3. Control variable $u_3(t)$: The asymptomatic population transitions to the symptomatic state at a rate denoted by γ_1, where ϕ represents the proportion of asymptomatic individuals who undergo this progression. Since treatment and isolation measures involve financial costs, policymakers must strategically manage these expenditures. To facilitate this optimization, the rate γ_1 is modeled as a time-dependent control variable, $u_3(t)$. In this context, u_3 represents interventions such as medical treatment or isolation efforts, which impact the progression from the asymptomatic to symptomatic states, in the context of model (1).

4. Control variable $u_4(t)$: Natural decay rate of the virus, ϵ is treated as a control variable $u_4(t)$.

The control variables $u_1(t), u_2(t), u_3(t)$, and $u_4(t)$ must be chosen from a set of allowable control functions defined by
$U = \{(u_1(t), u_2(t), u_3(t), u_4(t) \mid 0 \leq u_1(t) \leq u_{1\max},\ 0 \leq u_2(t) \leq u_{2\max},\ 0 \leq u_3(t) \leq u_{3\max},\ 0 \leq u_4(t) \leq u_{4\max}, t \in [t_0, t_f]\}$[38]. Here, $u_1(t)$,$u_2(t)$, $u_3(t)$, and $u_4(t)$ are measurable and bounded, and t_f is the final time for the intervention strategies. It is important to note that this final time t_f may vary for different diseases and applied interventions, depending on the goals of the control policy. So the following objective function is to minimize both the total number of infections and the related costs, which is expressed as

$$J(u) = \min \int_{t_0}^{t_f} \left(C + D_1 \frac{u_1^2}{2} + D_2 \frac{u_2^2}{2} + D_3 \frac{u_3^2}{2} + D_4 \frac{u_4^2}{2} \right) dt, \tag{11}$$

where $C = C_1 E + C_2 I_a + C_3 I + C_4 U - C_5 A, u = (u_1, u_2, u_3, u_4)$, and subject to constraints

$$\begin{cases} \frac{dS}{dt} &= \Lambda - \beta(1-u_1)(I+\eta I_a)S - \beta_1(1-u_1)SU + \lambda_0 A + \xi R - \frac{u_2 MS}{c+M} - \mu S \\ \frac{dA}{dt} &= \frac{u_2 MS}{c+M} - \lambda_0 A - \mu A \\ \frac{dE}{dt} &= \beta(1-u_1)(I+\eta I_a)S + \beta_1(1-u_1)SU - (k_2(1-\sigma) + k_1\sigma + \mu)E \\ \frac{dI_a}{dt} &= k_2(1-\sigma)E - u_3\phi I_a - \gamma_2(1-\phi)I_a - \mu I_a \\ \frac{dI}{dt} &= k_1\sigma E + u_3\phi I_a - \gamma_3 I - \delta I - \mu I \\ \frac{dR}{dt} &= \gamma_2(1-\phi)I_a + \gamma_3 I - \xi R - \mu R \\ \frac{dU}{dt} &= \theta_1 I_a + \theta_2 I - u_4 U \\ \frac{dM}{dt} &= r_1(1 - \frac{\theta A}{\omega + A})I - r_0(M - m_0). \end{cases} \tag{12}$$

We presume the initial circumstances:
$S(0) = S_0 > 0,\quad E(0) \geq 0,\quad I_a(0) \geq 0,\quad I(0) \geq 0,\quad A(0) = A_0 > 0,\quad R(0) \geq 0,\quad U(0) \geq 0.$ In the objective function, the constants C_1, C_2, C_3, C_4, and C_5 denote the weighting factors assigned to the exposed class, infected classes (I_a, I, and U), and the aware class, respectively. The time-dependent control variables u_1, u_2, u_3 and u_4 are associated with the quadratic costs $D_1 u_1^2, D_2 u_2^2, D_3 u_3^2$ and $D_4 u_4^2$, respectively, where the square terms indicate the severity of the costs.

The Filippov–Cesari Theorem [6] guarantees that the necessary conditions for achieving an optimal solution to the formulated optimal control problem are fulfilled. The Hessian matrix associated with the given cost functional is expressed as $\mathbf{D} = \text{diag}(D_1, D_2, D_3, D_4)$. Since this Hessian matrix is positive definite at all points, the objective functional $J(u_1, u_2, u_3, u_4)$ is strictly convex. Consequently, there exists a constant $D = \min D_1, D_2, D_3, D_4 > 0$ such that this lower bound applies to the integrand of the objective functional

$$\begin{aligned} &C + D_1\frac{u_1^2}{2} + D_2\frac{u_2^2}{2} + D_3\frac{u_3^2}{2} + D_4\frac{u_4^2}{2} \\ &\geq D\left(u_1^2 + u_2^2 + u_3^2 + u_4^2\right), \end{aligned}$$

holds if $E + I_a + I + A + U \geq 0$. We apply Pontryagin's maximum principle with the state variables $S = S^*, A = A^*, E = E^*, I_a = I_a^*, I = I^*, R = R^*, U = U^*, M = M^*$. We get the Hamiltonian function:

$$\begin{aligned} H =& C_1E^* + C_2I_a^* + C_3I^* + C_4U^* - C_5A^* + D_1\frac{u_1^2}{2} + D_2\frac{u_2^2}{2} + D_3\frac{u_3^2}{2} + D_4\frac{u_4^2}{2} \\ &+ \lambda_1\frac{dS}{dt} + \lambda_2\frac{dA}{dt} + \lambda_3\frac{dE}{dt} + \lambda_4\frac{dI_a}{dt} + \lambda_5\frac{dI}{dt} + \lambda_6\frac{dR}{dt} + \lambda_7\frac{dU}{dt} + \lambda_8\frac{dM}{dt}. \end{aligned} \tag{13}$$

The corresponding adjoint functions $\lambda_i, i = 1, 2, \ldots, 8$, satisfy the equations:

$$\begin{cases} \frac{d\lambda_1}{dt} &= -\frac{\partial H}{\partial S} \\ &= -\left(((1-u_1)\beta_1 U + (1-u_1)\beta(I + I_a\eta))(\lambda_2 - \lambda_1) + \frac{u_2(\lambda_5-\lambda_1)M}{M+c} - \lambda_1\mu\right); \\ \frac{d\lambda_2}{dt} &= -\frac{\partial H}{\partial A} \\ &= -(-C_4 + \lambda_0\lambda_1 - \lambda_5(\lambda_0 + \mu) - \frac{r_1\theta\lambda_8\omega I}{(A+\omega)^2}); \\ \frac{d\lambda_3}{dt} &= -\frac{\partial H}{\partial E} \\ &= -(C_1 + k_2(\lambda_2 - \lambda_3)(-1+\phi) + k_1\lambda_4\phi - \lambda_2(\mu + k_1\phi)); \\ \frac{d\lambda_4}{dt} &= -\frac{\partial H}{\partial I_a} \\ &= -(C_2 + (-1+u_1)\beta\eta(\lambda_1 - \lambda_2)S - \lambda_3\mu + \gamma_2(\lambda_3 - \lambda_6)(-1+\phi)) \\ &\quad -(\theta_1\lambda_7 - u_3(\lambda_3 - \lambda_4)\phi); \\ \frac{d\lambda_5}{dt} &= -\frac{\partial H}{\partial I} \\ &= -(C_3 + (-1+u_1)\beta(\lambda_1 - \lambda_2)S + \gamma_3(-\lambda_4 + \lambda_6) + \theta_2\lambda_7 - \lambda_4(\delta + \mu)) \\ &\quad -\left(r_1\lambda_8\left(1 - \frac{A\,\theta}{A+\omega}\right)\right); \\ \frac{d\lambda_6}{dt} &= -\frac{\partial H}{\partial R} \\ &= -(\lambda_1\xi + \lambda_6(\mu + \xi)); \\ \frac{d\lambda_7}{dt} &= -\frac{\partial H}{\partial U} \\ &= (1-u_1)\beta_1(\lambda_1 - \lambda_2)S + u_4\lambda_7; \\ \frac{d\lambda_9}{dt} &= -\frac{\partial H}{\partial M} \\ &= (\frac{cu_2S(\lambda_1-\lambda_5)}{(M+c)^2} + r_0\lambda_8). \end{cases}$$

Under the universality condition $\lambda_i(t_f) = 0$, and considering that for all control inputs u_i, where $i = 1, \ldots, 4$, the following condition holds:

$$\frac{\partial H}{\partial u_i} = 0,$$

The optimal control strategy, according to the appropriate variational principle, is determined as follows:

$$u_1^* = \min\left\{ \max\left(0, -\frac{(\beta I+\beta_1 U+\beta\eta I_a)(\lambda_1-\lambda_2)}{D_1}\right), u_{1\max}\right\},$$
$$u_2^* = \min\left\{ \max\left(0, \frac{(\lambda_1-\lambda_5)MS}{D_2(M+c)}\right), u_{2\max}\right\},$$
$$u_3^* = \min\left\{ \max\left(0, \frac{(\lambda_3-\lambda_4)\phi I_a}{D_4}\right), u_{3\max}\right\},$$
$$u_4^* = \min\left\{ \max\left(0, \frac{\lambda_7 U^*}{D_5}\right), u_{4\max}\right\}.$$

5.1 Numerical solution of the model with optimal control

In this subsection, we conduct numerical simulations of the optimal control model to investigate how different time-varying control strategies influence the dynamics of disease spread. The simulations are based on the parameter values listed in Table 2, with some parameters obtained through data fitting using COVID-19 data from India. The analysis is conducted assuming a total population of around 1.40 billion. An initial estimate for the control functions is proposed for the specified period. Additionally, we apply the forward-backward sweep method, as outlined in [6], to numerically simulate the optimal control solution.

The trajectories shown in Figures 9a–9d reveal how each control variable u_i (for $i = 1, 2, 3, 4$) uniquely influences the state variables E, I_a, I, and U. Solid lines represent the system's behavior without control, whereas dotted lines illustrate the impact of implementing control strategies. These interventions effectively reduce the number of infected individuals and the overall viral load, highlighting their success in significantly lowering the rate of virus introduction into the environment and limiting the progression into the in-

fected class I. Figure 10 presents the optimal control levels for u_1, u_2, u_3, and u_4 in the context of COVID-19 spread. In particular, Figure 10a shows that u_1 reaches its highest level between days 250 and 270, then gradually declines until day 300. Similarly, Figure 10b illustrates that u_2 peaks near day 290 and then slowly decreases up to day 300. Meanwhile, Figure 10c indicates that u_3 peaks between days 200 and 250 before tapering off by day 300. Lastly, Figure 10d shows u_4 reaching its maximum between days 270 and 290, then gradually declining until day 300.

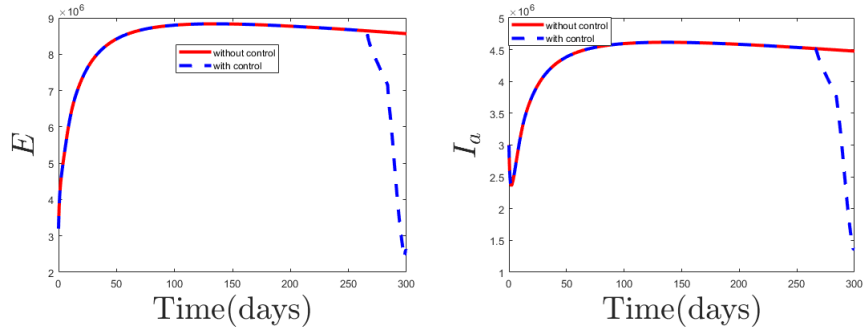

(a) Effect on E

(b) Effect on I_a

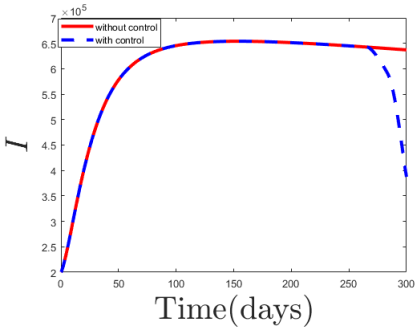

(c) Effect on I

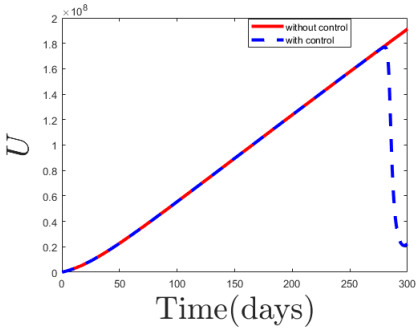

(d) Effect on U

Figure 9: Effect of control measures: u_1, u_2, u_3, u_4

To improve resource utilization and lower the costs associated with managing COVID-19 dynamics, we adopt selective strategies that concentrate on particular combinations of time-dependent control variables rather than employing all five control parameters simultaneously. This method allows us

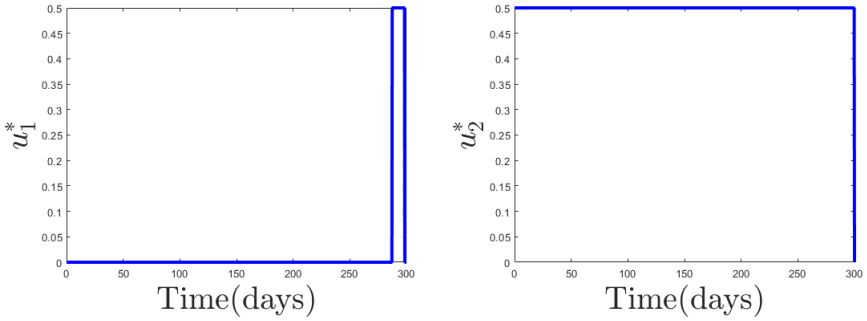

(a) Control parameter u_1^* (b) Control parameter u_2^*

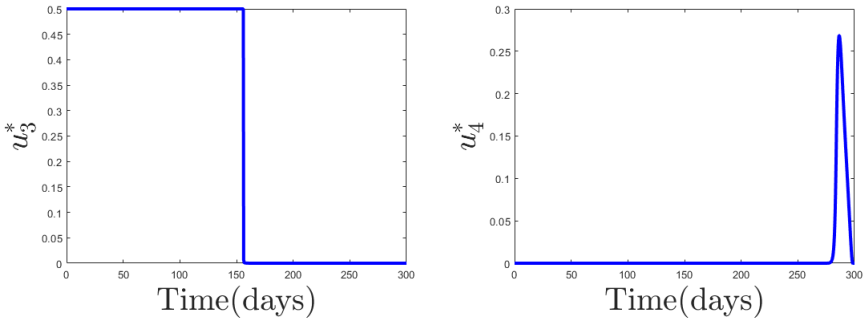

(c) Control parameter u_3^* (d) Control parameter u_4^*

Figure 10: Control profiles: u_1, u_2, u_3 and u_4

Table 4: Scenarios with their combination strategy

Scenario	**Strategies**
A	S-1. $(u_1 \neq 0, u_2 = 0, u_3 = 0, u_4 = 0)$
	S-2. $(u_1 = 0, u_2 \neq 0, u_3 = 0, u_4 = 0)$
	S-3. $(u_1 = 0, u_2 = 0, u_3 \neq 0, u_4 = 0)$
	S-4. $(u_1 \neq 0, u_2 \neq 0, u_3 \neq 0, u_4 = 0)$
B	S-5. $(u_1 = 0, u_2 = 0, u_3 = 0, u_4 \neq 0)$
C	S-6. $(u_1 \neq 0, u_2 \neq 0, u_3 \neq 0, u_4 \neq 0)$

to evaluate the impact of different control combinations (see Table 4), pro-

viding valuable insights into the trade-offs and cost-effectiveness of targeted interventions.

We assess three scenarios, A, B, and C, according to the control strategies outlined in Table 4 and illustrated in Figure 10. Scenario A explores the influence of control variables u_1, u_2, and u_3 while excluding u_4 (refer to Figures 11a–11d). Scenario B focuses on the effect of u_4 in the absence of u_1, u_2, and u_3 (see Figure 11e). Lastly, Scenario C examines the combined impact of all control variables u_1, u_2, u_3, and u_4 (Figure 11f).

Numerical simulations suggest that targeting infective groups (u_1, u_2, and u_3) in Scenario A is more effective in reducing disease transmission than implementing environmental controls (u_4) in Scenario B. Additionally, applying control measures to all infective groups simultaneously (Figures 11a–11d) yields a more significant impact compared to implementing them individually (Figures 11a–11c). Among the analyzed scenarios, Scenario C, which combines all control strategies, emerges as the most effective in limiting disease spread, as shown in Figure 11f.

Our analysis of optimal control indicates that successfully applying these strategies can greatly reduce transmission among vulnerable populations, leading to a marked decrease in the pandemic's overall impact.

6 Discussion and conclusion

The COVID-19 pandemic has presented significant public health challenges while exerting considerable economic pressure worldwide. With no pharmaceutical treatments initially available, nonpharmaceutical interventions like wearing face masks have been essential in curbing the virus's spread. Moreover, media coverage has played a key role in increasing public awareness and distributing critical information on preventive measures. This study examined the $SAEI_aIRUM$ model, which integrates nonlinear functional responses to capture the effects of media coverage influence.

We theoretically analyzed the model within the dynamical systems framework, ensuring the solutions remain positive and bounded. Furthermore, we explored the biological significance of the control reproduction number, which was derived using the next-generation matrix. The identified control repro-

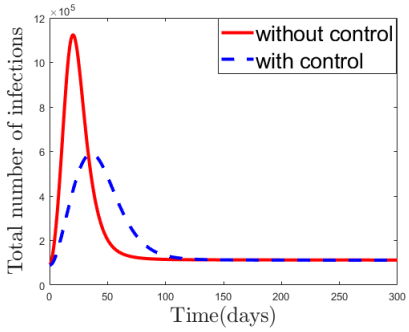

(a) S-1: control u_1 only

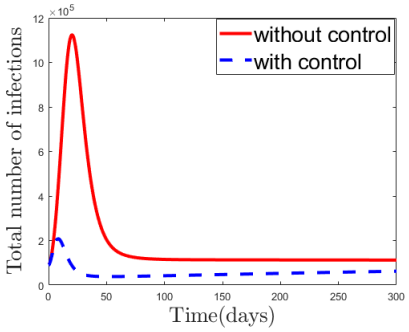

(b) S-2: control u_2 only

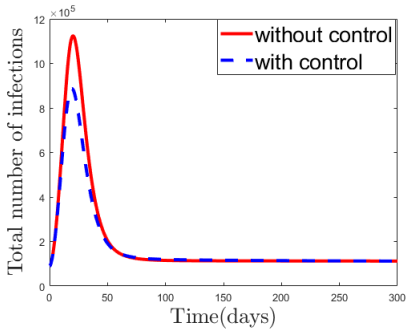

(c) S-3: control u_3 only

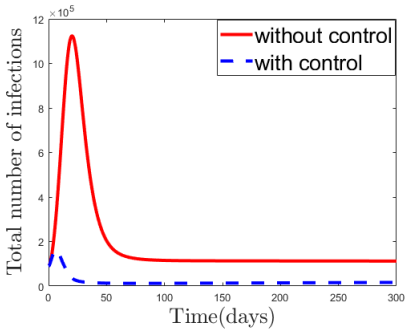

(d) S-5: u_1, u_2, u_3 only

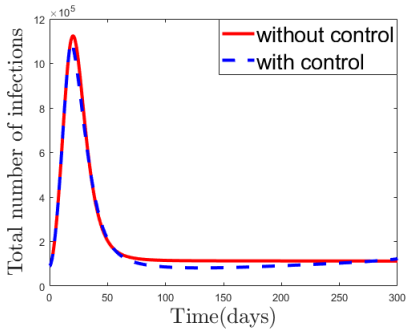

(e) S-5: u_4 only

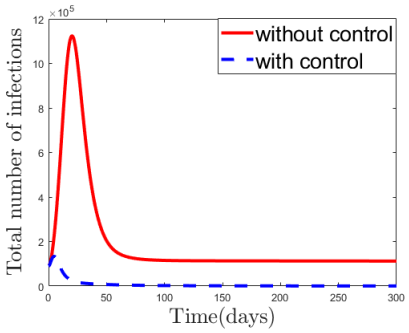

(f) S-6: u_1, u_2, u_3 and u_4

Figure 11: Effect of control u_1, u_2, u_3, u_4 and u_5 on total number of infections

duction number (R_c) and model equilibrium points include disease-free and

endemic states. Additionally, we examined the local stability of the DFE under the assumption that R_c is less than one.

Section 4 presents the numerical simulations of the proposed model, utilizing COVID-19 data from India, covering the period from March 30, 2020, to January 24, 2021, as obtained from Johns Hopkins University [27]. As depicted in Figure 3, our model demonstrates superior predictive accuracy compared to the Asamoah et al. [5] model, reinforcing our assertion that it provides the most precise forecasts. A numerical analysis examines the impact of various control parameters on disease prevalence. The practical implementation of nonpharmaceutical interventions (NPIs), such as wearing face masks and self-administering treatment, contributes to reducing the control reproduction number, as illustrated in Figure 7b. Figures 6a–6b demonstrate that increasing the values of λ results in a decline in the number of infected individuals. Furthermore, the gradual waning of immunity acquired through infection increases the risk of reinfection, underscoring the importance of booster vaccinations in maintaining immunity and mitigating disease transmission, as shown in Figure 7c. Conversely, Figures 8a–8b highlight the effects of environmental contamination. Figure 8c illustrates how variations in ϵ influence infection peaks, showing a decline as viral removal efforts intensify.

The control reproduction number (R_c) determines whether the disease persists or diminishes. A normalized sensitivity analysis (Figure 4) explores the influence of different parameters on R_c. Normalized forward sensitivity analyses indicate that the recruitment rate (Λ) has the most significant positive impact. In contrast, the proportion of susceptible individuals who become aware (λ) exerts the most substantial negative effect on R_c.

We enhanced the $SAEI_aIRUM$ model by embedding it within an optimal control framework, incorporating key interventions such as face masks, public awareness campaigns, medical treatment or isolation, and disinfection efforts. The impact of these measures was evaluated through simulations using the forward-backward sweep method. To assess the effectiveness and cost-efficiency of different strategies, we explored three distinct scenarios: Scenario A prioritizes managing infected individuals, Scenario B focuses on minimizing environmental contamination, and Scenario C combines both strategies.

Numerical simulations, illustrated in Figure 11, indicate that while Scenario A significantly reduces disease transmission compared to Scenario B, Scenario C, by combining all control measures, emerges as the most effective and cost-efficient strategy for controlling the spread of the disease.

Time delays significantly impact system dynamics, including delays in reporting confirmed cases caused by incubation periods and other influencing factors. Expanding this method could reveal more intricate dynamics in future research.

Declarations

Funding This study was conducted without financial support from any particular funding organization.

Data availability All the data used in this article can be accessed freely through the website https://data.humdata.org/dataset/novel-coronavirus-2019-ncov-cases#data-resources-0.

Author contribution Both authors contributed equally.

Conflict of interest No potential conflicts of interest are associated with this research.

References

[1] Alanazi, K.M. *The asymptotic spreading speeds of COVID-19 with the effect of delay and quarantine*, AIMS Math. 9(7) (2024), 19397–19413.

[2] Aldila, D. *Analyzing the impact of the media campaign and rapid testing for COVID-19 as an optimal control problem in East Java, Indonesia*, Chaos, Solitons Fractals, 141 (2020), 110364.

[3] Aldila, D., Khoshnaw, S.H.A., Safitri, E., Anwar, Y.R., Bakry, A.R.Q., Samiadji, B.M., Anugerah, D.A., Gh, M.F. A., Ayulani, I.D. and Salim, S.N. *A mathematical study on the spread of COVID-19 considering social distancing and rapid assessment: The case of Jakarta, Indonesia*, Chaos Solitons Fractals, 139 (2020), 110042.

[4] Anderson, R.M., Heesterbeek, H., Klinkenberg, D. and Hollingsworth, D.T. *How will country-based mitigation measures influence the course of the COVID-19 epidemic ?*, The Lancet, 395 (10228) (2020), 931–934.

[5] Asamoah, J.K.K., Owusu, M.A., Jin, Z., Oduro, F.T., Abidemi, A. and Gyasi, E.O. *Global stability and cost-effectiveness analysis of COVID-19 considering the impact of the environment: using data from Ghana*, Chaos, Solitons Fractals, 140 (2020), 110103.

[6] Atangana, A. and İğret, A.S. *Mathematical model of COVID-19 spread in Turkey and South Africa: theory, methods, and applications*, Adv. Differ. Equ. 2020(1) (2020), 1–89.

[7] Bajiya, V.P., Bugalia, S., Tripathi, J.P. and Martcheva, M. *Deciphering the transmission dynamics of COVID- 19 in India: optimal control and cost effective analysis*, J. Biol. Dyn. 16(1) (2022), 665–712.

[8] Baroudi, M., Laarabi, H., Zouhri, S., Rachik, M. and Abta, A. *Stochastic optimal control model for COVID-19: mask wearing and active screening/testing*, J. Appl. Math. Comput. 70(6) (2024), 6411–6441.

[9] BBC, News https://www.bbc.com/news/world-asia-india-52077395 (Accessed: June, 2022).

[10] Birkhoff, G. and Rota, G. *Ordinary Differential Equations*, Wiley, United Kingdom, 1978.

[11] Castillo-Chavez, C. and Song, B. *Dynamical models of tuberculosis and their applications*, Math. Biosci. Eng. 1(2) (2004), 361–404.

[12] Chang, X., Liu, M., Jin, Z. and Wang, J. *Studying on the impact of media coverage on the spread of COVID-19 in Hubei Province, China,* Math. Biosci. Eng. 17(4) (2020), 3147–3159.

[13] Chen, K., Pun, C.S. and Wong, H.Y. *Efficient social distancing during the COVID-19 pandemic: integrating economic and public health considerations*, European J. Oper. Res. 304(1) (2023), 84–98.

[14] Chen, N., Zhou, M., Dong, X., Qu, J., Gong, F., Han, Y., Qiu, Y., Wang, J., Liu, Y., Wei, Y. and Xia, J.A. *Epidemiological and clinical characteristics of 99 cases of 2019 novel coronavirus pneumonia in Wuhan, China: a descriptive study*, The Lancet, 395(10223) (2020), 507–513.

[15] Chen, T., Li, Z. and Zhang, G. *Analysis of a COVID-19 model with media coverage and limited resources*, Math. Biosci. Eng. 21(4) (2024), 5283–5307.

[16] Cheneke, K. *Optimal control analysis for modeling HIV transmission*, Iran. J. Numer. Anal. Optim. 13(4) (2023), 747–762.

[17] Cucinotta, D. and Vanelli, M. *WHO declares COVID-19 a pandemic*, Acta Biomed. 91(1) (2020), 157.

[18] d'Onofrio, A., Iannelli, M., Manfredi, P. and Marinoschi, G. *Epidemic control by social distancing and vaccination: optimal strategies and remarks on the COVID-19 Italian response policy*, Math. Biosci. Eng. 21(7) (2024), 6493–6520.

[19] Dwivedi, S., Perumal, S.K., Kumar, S., Bhattacharyya, S. and Kumari, N. *Impact of cross border reverse migration in Delhi- UP region of India during COVID-19 lockdown*, Comput. Math. Biophys. 11 (2023), 1–26.

[20] Gholami, M., Mirhosseini, A.S. and Heidari, A. *Designing a sliding mode controller for a class of multi-controller COVID-19 disease model*, Iran. J. Numer. Anal. Optim. 15(1) (2025), 27–53.

[21] Ghosh, I., Tiwari, P.K., Samanta, S., Elmojtaba, I.M., Al-Salti, N. and Chattopadhyay, J. *A simple SI-type model for HIV/AIDS with media and self-imposed psychological fear*, Math. Biosci. 306 (2018), 160–169.

[22] Government of India https://www.mygov.in/covid-19 (Accessed: June, 2022).

[23] Guo, Y. and Li, T. *Modeling the competitive transmission of the Omicron strain and Delta strain of COVID-19*, J. Math. Anal. Appl. 526(2) (2023), 127283.

[24] Gupta, S., Rajoria, Y.K. and Sahu, G.P. *Mathematical Modelling on Dynamics of Multi-variant SARS-CoV-2 Virus: Estimating Delta and Omicron Variant Impact on COVID-19*, IJAM 55(1) (2025), 180–188.

[25] Hao, J., Huang, L., Liu, M. and Ma, Y. *Analysis of the COVID-19 model with self-protection and isolation measures affected by the environment*, Math. Biosci. Eng. 21(4) (2024), 4835–4852.

[26] Huang, C., Wang, Y., Li, X., Ren, L., Zhao, J., Hu, Y., Zhang, L., Fan, G., Xu, J., Gu, X. and Cheng, Z. *Clinical features of patients infected with 2019 novel coronavirus in Wuhan, China*, The lancet, 395(10223) (2020), 497–506.

[27] Humanitarian Data Exchange. Novel Coronavirus 2019 (COVID-19) Cases https://data.humdata.org/dataset/novel-coronavirus-2019-ncov-cases#data-resources-0 (Accessed: June, 2023).

[28] Iboi, E., Sharomi, O.O., Ngonghala, C. and Gumel, A.B. *Mathematical modeling and analysis of COVID-19 pandemic in Nigeria*, MedRxiv, (2020), 1–24.

[29] Kahn, J.S. and McIntosh, K. *History and recent advances in coronavirus discovery* Pediatr. Infect. Dis. J. 24(11) (2005), S223–S227.

[30] Killerby, M.E., Biggs, H.M., Midgley, C.M., Gerber, S.I. and Watson, J.T. *Middle East respiratory syndrome coronavirus transmission* Emerg. Infect. Dis. 26(2) (2020), 191.

[31] Koura, A.F., Raslan, K.R., Ali, K.K. and Shaalan, M.A. *A numerical investigation for the COVID-19 spatiotemporal lockdown-vaccination model*, Comput. Methods Differ. Equ. 12(4) (2024), 669–686.

[32] Kumar, A., Srivastava, P.K., Dong, Y., and Takeuchi, Y. *Optimal control of infectious disease: Informationinduced vaccination and limited treatment*, Phys. A: Stat. Mech. Appl. 542 (2020), 123196.

[33] Kurkina, E. and Koltsova, E. *Mathematical modeling of the propagation of Covid-19 pandemic waves in the World*, Comput. Math. Model. 32(2021), 147–170.

[34] Lakhal, M., Taki, R., El F.M. and El, G.T. *Quarantine alone or in combination with treatment measures to control COVID-19*, J. Anal. 31(4) (2023), 2347–2369.

[35] LaSalle, J.P. *Stability theory and invariance principles*, Elsevier, New York, 1976.

[36] Li, Q., Guan, X., Wu, P., Wang, X., Zhou, L., Tong, Y., Ren, R., Leung, K.S., Lau, E.H., Wong, J.Y. and Xing, X. *Early transmission dynamics in Wuhan, China, of novel coronavirus infected pneumonia*, N. Engl. J. Med. 382(13) (2020), 1199–1207.

[37] Liu, J. and Wang, X.S. *Dynamic optimal allocation of medical resources: a case study of face masks during the first COVID-19 epidemic wave in the United States*, Math. Biosci. Eng. 20(7) (2023), 12472–12485.

[38] Martcheva, M. *An introduction to mathematical epidemiology*, Springer, United States, 2015.

[39] Memon, Z., Qureshi, S. and Memon, B.R. *Assessing the role of quarantine and isolation as control strategies for COVID-19 outbreak: a case study*, Chaos Solitons Fractals, 144 (2021), 110655.

[40] Misra, A., Sharma, A. and Shukla, J. *Modeling and analysis of effects of awareness programs by media on the spread of infectious diseases*, Math. Comput. Model. 53(5-6) (2011), 1221–1228.

[41] Misra, A.K., Rai, R.K. and Takeuchi, Y. *Modeling the control of infectious diseases: Effects of TV and social media advertisements*, Math. Biosci. Eng. 15(6) (2018), 1315–1343.

[42] Rai, R.K., Khajanchi, S., Tiwari, P.K., Venturino, E. and Misra, A.K. *Impact of social media advertisements on the transmission dynamics of COVID-19 pandemic in India*, J. Appl. Math. Comput. (2022), 1–26.

[43] Sahu, G.P. and Dhar, J. *Analysis of an SVEIS epidemic model with partial temporary immunity and saturation incidence rate*, Appl. Math. Model. 36(3) (2012), 908–923.

[44] Sahu, G.P. and Dhar, J. *Dynamics of an SEQIHRS epidemic model with media coverage, quarantine and isolation in a community with preexisting immunity*, J. Math. Anal. Appl. 421(2) (2015), 1651–1672.

[45] Sardar, T., Nadim, S.k.S., Rana, S. and Chattopadhyay, J. *Assessment of lockdown effect in some states and overall India: a predictive mathematical study on COVID-19 outbreak*, Chaos Solitons Fractals, 139 (2020), 1-10.

[46] Sarkar, K., Mondal, J. and Khajanchi, S. *How do the contaminated environment influence the transmission dynamics of COVID-19 pandemic?*, Eur. Phys. J: Spec. Top. 231(18-20) (2022), 3697–3716.

[47] Senapati, A., Rana, S., Das, T. and Chattopadhyay, J. *Impact of intervention on the spread of COVID-19 in India: A model based study*, J. Theor. Biol. 523 (2021) 110711.

[48] Sooknanan, J. and Comissiong, D. *Trending on social media: integrating social media into infectious disease dynamics*, Bull. Math. Biol. 82(7) (2020), 86.

[49] Sooknanan, J. and Mays, N. *Harnessing social media in the modelling of pandemics challenges and opportunities*, Bull. Math. Biol. 83(5) (2021), 57.

[50] Srivastav, A.K., Tiwari, P.K., Srivastava, P.K., Ghosh, M. and Kang, Y. *A mathematical model for the impacts of face mask, hospitalization and quarantine on the dynamics of COVID-19 in India: deterministic vs. stochastic*, Math. Biosci. Eng. 18(1) (2021), 182–213.

[51] Su, S., Wong, G., Shi, W., Liu, J., Lai, A.C.K., Zhou, J., Liu, W., Bi, Y. and Gao, G.F. *Epidemiology, genetic recombination, and pathogenesis of coronaviruses*, Trends Microbiol. 24(6) (2016), 490–502.

[52] Sun, D., Li, Y., Teng, Z., Zhang, T., and Lu, J. *Dynamical properties in an SVEIR epidemic model with age-dependent vaccination, latency, infection, and relapse*, Math. Methods Appl. Sci. 44(17) (2021), 12810–12834.

[53] Thakur, A.S. and Sahu, G.P. *Modeling the COVID-19 Dynamics with Omicron Variant, Non-pharmaceutical Interventions, and Environmental Contamination* Differ. Equations Dyn. Syst. (2025), 1–25.

[54] The Indian Express https://indianexpress.com/article/coronavirus/coronavirus-india-infection-rate-china-6321154/ (Accessed: June, 2023).

[55] Van den Driessche, P. and Watmough, J. *Reproduction numbers and subthreshold endemic equilibria for compartmental models of disease transmission*, Math. Biosci. 180(1-2) (2002), 29–48.

[56] Van Doremalen, N., Bushmaker, T., Morris, D.H., Holbrook, M.G., Gamble, A., Williamson, B.N., Tamin, A., Harcourt, J.L., Thornburg, N.J., Gerber, S.I. and Lloyd-Smith, J.O. *Aerosol and surface stability of SARS-CoV- 2 as compared with SARS-CoV-1*, N. Engl. J. Med. 382(16) (2020), 1564–1567.

[57] Wang, W. and Ruan, S. *Bifurcation in an epidemic model with constant removal rate of the infectives*, J. Math. Anal. Appl. 291(2) (2004), 775–793.

[58] Wang, X., Liang, Y., Li, J. and Liu, M. *Modeling COVID-19 transmission dynamics incorporating media coverage and vaccination*, Math. Biosci. Eng. 20 (2023), 10392–10403.

[59] Wardeh, M., Baylis, M. and Blagrove, M. S. *Predicting mammalian hosts in which novel coronaviruses can be generated*, Nat. Commun. 12(1) (2021), 780.

[60] Willman, M., Kobasa, D. and Kindrachuk, J.A. *Comparative analysis of factors influencing two outbreaks of Middle Eastern respiratory syndrome (MERS) in Saudi Arabia and South Korea*, Viruses 11(12) (2019), 1119.

[61] Yuan, R., Ma, Y., Shen, C., Zhao, J., Luo, X. and Liu, M. *Global dynamics of COVID-19 epidemic model with recessive infection and isolation*, Math. Biosci. Eng. 18(2) (2021), 1833–1844.

[62] Yuan, Y. and Li, N. *Optimal control and cost-effectiveness analysis for a COVID-19 model with individual protection awareness*, Phys. A: Stat. Mech. Appl. 603 (2022), 127804.

[63] Zhao, S., Lin, Q., Ran, J., Musa, S.S., Yang, G., Wang, W., Lou, Y., Gao, D., Yang, L., He, D. and Wang, M.H. *Preliminary estimation of the basic reproduction number of novel coronavirus (2019-nCoV) in China, from 2019 to 2020: A data driven analysis in the early phase of the outbreak*, Int. J. Inf. Dis. 92 (2020), 214–217.